Certifying the Nonexistence of Feasible Paths Between Power System Operating Points

Mohammad Rasoul Narimani,* Katherine R. Davis,** and Daniel K. Molzahn[†]

Abstract—By providing the optimal operating point that satisfies both the power flow equations and engineering limits, the optimal power flow (OPF) problem is central to power systems operations. While extensive research has focused on computing high-quality OPF solutions, assessing the feasibility of transitioning between operating points remains challenging since the feasible spaces of OPF problems may consist of multiple disconnected components. It is not possible to transition between operating points in different disconnected components without violating OPF constraints. To identify such situations, this paper introduces an algorithm for certifying the infeasibility of transitioning between two operating points within an OPF feasible space. As an indication of potential disconnectedness, the algorithm first seeks an infeasible point on the line connecting a pair of feasible points. The algorithm then certifies disconnectedness by using convex relaxation and bound tightening techniques to show that all points on the plane that is normal to this line are infeasible. Using this algorithm, we provide the first certifications of disconnected feasible spaces for a variety of OPF test cases.

I. INTRODUCTION

Optimal power flow (OPF) is a crucial problem in power system operations. This problem seeks an optimal operating point within a feasible space determined by the power flow equations and inequality constraints that limit voltage magnitudes, line flows, and generator outputs. OPF feasible spaces are nonconvex and may consist of multiple disconnected components [1], making the OPF problem NP-hard in general [2].

A wide variety of local optimization and approximation algorithms have been applied to OPF problems [3], [4]. Many convex relaxations have also been developed to bound optimal objective values, certify infeasibility, and in some cases, obtain globally optima [4]. An OPF problem's difficulty is closely related to the convexity characteristics of the feasible space. In this context, many research efforts have studied the geometry of the OPF feasible spaces, e.g., [1], [4]–[10].

The growth in fluctuating renewable generation motivates the need to manage increasingly frequent transitions between operating points to avoid large constraint violations (e.g., voltages and flows exceeding limits). There is limited literature on this topic. Prior work focuses on computing feasible paths between operating points within non-convex OPF feasible spaces [11]–[13]. Using power flow linearizations, related work in [14], [15] seeks the fewest control actions necessary to actuate a transition between operating points. However, the failure of existing algorithms to identify a feasible path does not guarantee that no path exists, i.e., they do not ensure that the initial and target operating points are necessarily in different disconnected components of the OPF feasible space.

In this context, we propose an algorithm which certifies that the feasible space of an OPF problem is disconnected. This algorithm contributes to the literature on the characteristics of OPF feasible spaces (e.g., [1], [4]–[10]) and identifies when feasible path algorithms such as [11]–[13] will necessarily fail. This avoids the computational effort of running path finding algorithms in situations where no feasible path exists. Moreover, certifying the disconnectedness of an OPF feasible space can inform operators of situations where constraint violations are unavoidable during the transition to a target operating point. As large constraint violations can damage equipment or trigger protection systems, this would help operators know when to use, e.g., decomposition and convex restriction methods [16] to identify a target operating point that is within the same component of the feasible space as the initial point.

Our proposed algorithm leverages concepts from [9] which identifies and characterizes non-convexities within OPF feasible spaces. The algorithm in [9] searches for a pair of feasible points connected by a line segment containing an infeasible point. The existence of such points certifies the presence of a non-convex region within an OPF problem's feasible space, but does not necessarily indicate that the feasible space is disconnected. Note that the causes of non-convexities in OPF feasible spaces are empirically investigated in [8], with results showing that non-convexities are often associated with binding lower bounds on voltage magnitudes and reactive generation.

The algorithm proposed in this paper first uses the approach in [9] to identify two candidate operating points which may be in different disconnected components due to the presence of an infeasible point between them. Our algorithm then formulates an optimization problem which augments the OPF constraints with a constraint restricting its solution to a plane that is perpendicular to the line connecting the two feasible points and passes through the previously identified infeasible point. Infeasibility of this optimization problem certifies that the OPF problem's feasible space is disconnected. To prove infeasibility, we relax this optimization problem using the Quadratic Convex (QC) power flow relaxation [17] and apply optimization-based bound tightening techniques [18]–[21]. To the best of our knowledge, this is the first algorithm that can rigorously identify the presence of disconnected components in OPF feasible spaces. Our numerical results show that several challenging OPF test cases have disconnected feasible spaces.

This paper is organized as follows. Section II reviews the OPF formulation. Section III describes the QC relaxation and optimization-based bound tightening. Section IV presents the proposed algorithm for determining the disconnectedness of OPF feasible spaces. Section V empirically demonstrates this

algorithm. Section VI concludes the paper.

II. OPTIMAL POWER FLOW OVERVIEW

This section overviews the AC OPF problem. Consider an n-bus system, where $\mathcal{N} = \{1, \ldots, n\}$, $\mathcal{G}$, and $\mathcal{L}$ are the sets of buses, generators, and lines. Let $P_{d,i} + \mathbf{j}Q_{d,i}$ and $P_{g,i} + \mathbf{j}Q_{g,i}$ represent the active and reactive load demand and generation, respectively, at bus $i \in \mathcal{N}$, where $\mathbf{j} = \sqrt{-1}$. Let $g_{sh,i} + \mathbf{j}b_{sh,i}$ denote the shunt admittance at bus i. Let V_i and θ_i represent the voltage magnitude and angle at bus $i \in \mathcal{N}$. For each generator $i \in \mathcal{G}$, define a quadratic generation cost function with coefficients $c_{2,i} \geqslant 0$, $c_{1,i}$, and $c_{0,i}$. Denote $\theta_{lm} = \theta_l - \theta_m$. Specified upper and lower limits are denoted by $(\overline{\cdot})$ and $(\underline{\cdot})$, respectively. Buses $i \in \mathcal{N}\backslash\mathcal{G}$ have generation limits set to zero.

Each line $(l, m) \in \mathcal{L}$ is modeled as a Π circuit with mutual admittance $g_{lm} + \mathbf{j}b_{lm}$ and shunt admittance $\mathbf{j}b_{sh,lm}$. (Our approach is applicable to more general line models, such the MATPOWER [22] model that allows for off-nominal tap ratios and non-zero phase shifts.) Let p_{lm}, q_{lm}, and $\overline{s}_{lm}$ represent the active and reactive power flows and the maximum apparent power flow limit on the line that connects buses l and m.

Using these definitions, the OPF problem is

$$\min \quad \sum_{i \in \mathcal{G}} c_{2i} \left(P_{g,i}\right)^2 + c_{1i} P_{g,i} + c_{0i} \tag{1a}$$

$$\text{subject to} \quad (\forall i \in \mathcal{N}, \ \forall (l, m) \in \mathcal{L})$$

$$P_{g,i} - P_{d,i} = g_{sh,i} V_i^2 + \sum_{\substack{(l,m)\in\mathcal{L} \\ \text{s.t. } l=i}} p_{lm} + \sum_{\substack{(l,m)\in\mathcal{L} \\ \text{s.t. } m=i}} p_{ml}, \tag{1b}$$

$$Q_{g,i} - Q_{d,i} = -b_{sh,i} V_i^2 + \sum_{\substack{(l,m)\in\mathcal{L} \\ \text{s.t. } l=i}} q_{lm} + \sum_{\substack{(l,m)\in\mathcal{L} \\ \text{s.t. } m=i}} q_{ml}, \tag{1c}$$

$$\theta_{ref} = 0, \tag{1d}$$

$$\underline{P}_{g,i} \leqslant P_{g,i} \leqslant \overline{P}_{g,i}, \quad \underline{Q}_{g,i} \leqslant Q_{g,i} \leqslant \overline{Q}_{g,i}, \tag{1e}$$

$$\underline{V}_i \leqslant V_i \leqslant \overline{V}_i, \quad \underline{\theta}_{lm} \leqslant \theta_{lm} \leqslant \overline{\theta}_{lm}, \tag{1f}$$

$$p_{lm} = g_{lm} v_l^2 - g_{lm} V_l V_m \cos\left(\theta_{lm}\right) - b_{lm} V_l V_m \sin\left(\theta_{lm}\right), \tag{1g}$$

$$q_{lm} = -\left(b_{lm} + b_{sh,lm}/2\right) V_l^2 + b_{lm} V_l V_m \cos\left(\theta_{lm}\right) - g_{lm} V_l V_m \sin\left(\theta_{lm}\right), \tag{1h}$$

$$\left(p_{lm}\right)^2 + \left(q_{lm}\right)^2 \leqslant \left(\overline{s}_{lm}\right)^2, \left(p_{ml}\right)^2 + \left(q_{ml}\right)^2 \leqslant \left(\overline{s}_{lm}\right)^2. \tag{1i}$$

The objective (1a) minimizes the generation cost. Constraints (1b) and (1c) enforce power balance at each bus. Constraint (1d) sets the angle reference. Constraints (1e)–(1f) limit the power generation, voltage magnitudes, and angle differences. Constraints (1g)–(1h) relate the voltages and power flows on each line, and (1i) limits apparent power flows.

III. REVIEW OF THE QC RELAXATION AND OPTIMIZATION-BASED BOUND TIGHTENING

We next review the QC relaxation [17] and optimization-based bound tightening [18]–[21] that underlie our algorithm.

A. Formulation of the QC Relaxation

The QC relaxation convexifies the OPF problem (1) by enclosing non-convex terms in convex envelopes. This relaxation defines new variables w_{ii}, w_{lm}, c_{lm}, and s_{lm} for products of voltage magnitudes and products of voltage magnitudes and trigonometric terms, i.e., $V_l V_m \cos(\theta_{lm})$ and $V_l V_m \sin(\theta_{lm})$:

$$w_{ii} = V_i^2, \forall i \in \mathcal{N}, \quad w_{lm} = V_l V_m, \quad c_{lm} = w_{lm} \cos\left(\theta_{lm}\right),$$

$$s_{lm} = w_{lm} \sin\left(\theta_{lm}\right), \ \forall (l, m) \in \mathcal{L}. \tag{2}$$

For every $(l, m) \in \mathcal{L}$, these definitions imply the following relationships among the variables w_{ll}, c_{lm}, and s_{lm}:

$$c_{lm}^2 + s_{lm}^2 = w_{ll} w_{mm}, \tag{3a}$$

$$c_{lm} = c_{ml}, \quad s_{lm} = -s_{ml}. \tag{3b}$$

Following [23], (3a) is relaxed to a convex second-order cone constraint by replacing the equality with an inequality:

$$c_{lm}^2 + s_{lm}^2 \leqslant w_{ll} w_{mm}. \tag{4}$$

The QC relaxation encloses the squared and bilinear product terms in convex envelopes, shown here as set-valued functions:

$$\langle x^2 \rangle^T = \begin{cases} \check{x} : \begin{cases} \check{x} \geqslant x^2, \\ \check{x} \leqslant \left(\overline{x} + \underline{x}\right) x - \overline{x}\underline{x}. \end{cases} \end{cases} \tag{5a}$$

$$\langle xy \rangle^M = \begin{cases} \widetilde{xy} : \begin{cases} \widetilde{xy} \geqslant \underline{x}y + \underline{y}x - \underline{x}\underline{y}, \\ \widetilde{xy} \geqslant \overline{x}y + \overline{y}x - \overline{x}\overline{y}, \\ \widetilde{xy} \leqslant \underline{x}y + \overline{y}x - \underline{x}\overline{y}, \\ \widetilde{xy} \leqslant \overline{x}y + \underline{y}x - \overline{x}\underline{y}. \end{cases} \end{cases} \tag{5b}$$

Here, $\check{x}$ and $\widetilde{xy}$ stand for "dummy" variables symbolizing their respective sets. The envelope $\langle x^2 \rangle^T$ is the convex hull of the square function. The McCormick envelope denoted as $\langle xy \rangle^M$ is the convex hull of a bilinear product [24].

The QC relaxation additionally uses convex envelopes $\langle \sin(x) \rangle^S$ and $\langle \cos(x) \rangle^C$ for the trigonometric functions:

$$\langle \sin(x) \rangle^S =$$
$$\begin{cases} \check{S} : \begin{cases} \check{S} \leqslant \cos\left(\frac{x^m}{2}\right)\left(x - \frac{x^m}{2}\right) + \sin\left(\frac{x^m}{2}\right), \\ \check{S} \geqslant \cos\left(\frac{x^m}{2}\right)\left(x + \frac{x^m}{2}\right) - \sin\left(\frac{x^m}{2}\right), \\ \check{S} \geqslant \frac{\sin(\underline{x}) - \sin(\overline{x})}{\underline{x} - \overline{x}}\left(x - \underline{x}\right) + \sin\left(\underline{x}\right) \text{ if } \underline{x} \geqslant 0, \\ \check{S} \leqslant \frac{\sin(\underline{x}) - \sin(\overline{x})}{\underline{x} - \overline{x}}\left(x - \underline{x}\right) + \sin\left(\underline{x}\right) \text{ if } \overline{x} \leqslant 0. \end{cases} \end{cases} \tag{6a}$$

$$\langle \cos(x) \rangle^C =$$
$$\begin{cases} \check{C} : \begin{cases} \check{C} \leqslant 1 - \frac{1 - \cos(x^m)}{(x^m)^2} x^2, \\ \check{C} \geqslant \frac{\cos(\underline{x}) - \cos(\overline{x})}{\underline{x} - \overline{x}}\left(x - \underline{x}\right) + \cos\left(\underline{x}\right). \end{cases} \end{cases} \tag{6b}$$

Here, $x^m = \max(|\underline{x}|, |\overline{x}|)$. The variables $\check{S}$ and $\check{C}$ are placeholders for their respective sets. When $-90° < \underline{x} < \overline{x} < 90°$, bounds on the sine and cosine functions are as follows:

$$\underline{s} = \sin\left(\underline{x}\right) \leqslant \sin(x) \leqslant \overline{s} = \sin\left(\overline{x}\right), \tag{7a}$$

$$\underline{c} = \min\left(\cos(\underline{x}), \cos(\overline{x})\right) \leqslant \cos(x)$$

$$\leqslant \overline{c} = \begin{cases} \max\left(\cos(\underline{x}), \cos(\overline{x})\right), \text{ if } \text{sign}\left(\underline{x}\right) = \text{sign}\left(\overline{x}\right), \\ 1, \text{ otherwise.} \end{cases} \tag{7b}$$

With a slight abuse of notation, the QC relaxation substitutes the square, product, and trigonometric terms in (1) with the variables w_{ii}, w_{lm}, c_{lm}, and s_{lm} in these envelopes as follows:

$$\min \quad \sum_{i \in \mathcal{G}} c_{2i} \left(P_{g,i}\right)^2 + c_{1i} P_{g,i} + c_{0i} \tag{8a}$$

$$\text{subject to} \quad (\forall i \in \mathcal{N}, \ \forall (l, m) \in \mathcal{L})$$

$$P_{g,i} - P_{d,i} = g_{sh,i} w_{ii} + \sum_{\substack{(l,m)\in\mathcal{L} \\ \text{s.t. } l=i}} p_{lm} + \sum_{\substack{(l,m)\in\mathcal{L} \\ \text{s.t. } m=i}} p_{ml}, \tag{8b}$$

$$Q_{g,i} - Q_{d,i} = -b_{sh,i}\, w_{ii} + \sum_{\substack{(l,m)\in\mathcal{L} \\ \text{s.t. } l=i}} q_{lm} + \sum_{\substack{(l,m)\in\mathcal{L} \\ \text{s.t. } m=i}} q_{ml}, \qquad (8c)$$

$$(\underline{V}_i)^2 \leqslant w_{ii} \leqslant (\overline{V}_i)^2, \qquad (8d)$$

$$p_{lm} = g_{lm} w_{ll} - g_{lm} c_{lm} - b_{lm} s_{lm}, \qquad (8e)$$

$$q_{lm} = -(b_{lm} + b_{sh,lm}/2)\, w_{ii} + b_{lm} c_{lm} - g_{lm} s_{lm}, \qquad (8f)$$

$$w_{ii} \in \left\langle V_i^2 \right\rangle^T,\, w_{lm} \in \left\langle V_l V_m \right\rangle^M,\, c_{lm} \in \left\langle w_{lm} \left\langle \cos(\theta_{lm}) \right\rangle^C \right\rangle^M,$$

$$s_{lm} \in \left\langle w_{lm} \left\langle \sin(\theta_{lm}) \right\rangle^S \right\rangle^M, \qquad (8g)$$

$$\text{Equations (1d)–(1f), (1i), (3b), (4).} \qquad (8h)$$

Note that the product terms in (1g) and (1h) are addressed in (8g) through a recursive application of McCormick envelopes (5b). The optimization problem (8) is a second-order cone program (SOCP), which is convex and can be solved efficiently using commercial tools (e.g., Gurobi, Mosek, etc.).

Convex relaxations have several complementary advantages over applying local optimization methods to the non-convex OPF problem (1) [4]. In our context, we leverage the fact that infeasibility of the QC relaxation (8) is sufficient to ensure infeasibility of the original non-convex OPF problem (1). In fact, convex relaxations are the only approach capable of rigorously certifying infeasibility of non-convex OPF problems.

B. Bound Tightening

The QC relaxation's tightness is closely linked to the precision of the bounds on voltage magnitudes ($\underline{V}_i$, $\overline{V}_i$), and angle differences ($\underline{\theta}_{lm}$, $\overline{\theta}_{lm}$). The dataset's values for these limits are often much larger than what is actually attainable considering the limitations implicit from other constraints. In other words, some limits are never binding. Leveraging this insight, algorithms focused on enhancing bound accuracy provide tighter bounds that enhance the QC relaxation's quality [18]–[21].

We use the optimization-based bound tightening algorithm from [18]. This iterative algorithm minimizes and maximizes each squared voltage magnitude and angle difference variable while enforcing the QC relaxation's constraints. To illustrate, we next examine the upper voltage limit at bus 1:

$$w_{11}^* = \max \quad w_{11} \quad \text{subject to} \quad (8b)\text{–}(8h). \qquad (9)$$

The value w_{11}^* establishes an upper limit on the maximum attainable value of $(V_1)^2$ within the feasible space. If w_{11}^* is less than $(\overline{V}_1)^2$, then (9) yields a smaller value of $\sqrt{w_{11}^*}$, serving as a tighter upper bound for V_1, thereby tightening the QC relaxation. As the act of tightening a bound on any particular variable may improve the achievable bounds for other variables, the bound tightening procedure follows an iterative procedure until no further bounds can be refined.

Improving the variable bounds tightens the feasible space of the relaxed OPF problem such that the relaxation is capable of certifying infeasibility for a broader set of OPF problems. Importantly, since the QC relaxation constraints enforced in (9) admit all feasible points for (1), note that the tightened bounds will never cut off portions of the original non-convex OPF problem's feasible space. Thus, infeasibility of the bound-tightened QC relaxation still ensures infeasibility of the original non-convex OPF problem (1). As described in the next section, we leverage this in our algorithm for certifying the presence of disconnected components in OPF feasible spaces.

IV. An Algorithm for Certifying Disconnectedness of an OPF Feasible Space

This section presents our algorithm for certifying the presence of disconnected components in the feasible space of OPF problems. We first summarize our prior method from [9] which identifies a pair of feasible operating points which have an infeasible point in between. We then describe our proposed algorithm for using these points to certify disconnectedness.

A. Identifying Non-Convexities in OPF Feasible Spaces

To identify two feasible operating points with an infeasible point in between, we rely on the concept of convexity. A feasible space is convex if and only if it includes all points along the line segments that connect every pair of feasible points. We utilize the algorithm from [9] to locate an infeasible point, denoted as point C, on the line connecting two feasible points, denoted as points A and B, within the feasible space of the OPF problem. Fig. 1 provides illustrative examples of convexity characteristics for both convex and non-convex sets.

In the domain of active power generation and voltage magnitudes, any point on the line segment connecting points A and B has active power generation at non-slack generator buses described by the expression $\lambda P_g^A + (1 - \lambda) P_g^B$, where λ is a scalar value in the range [0,1]. Similarly, the generator bus voltage magnitudes along this segment are characterized by $\lambda V^A + (1 - \lambda) V^B$. To identify non-convexity, the method in [9] seeks values for P_g^A, P_g^B, V^A, V^B, and λ such that:

- There exist power flow solutions corresponding to P_g^A, V^A and P_g^B, V^B that are feasible for *all* OPF constraints (1b)–(1i), including voltage, reactive power, and flow limits.
- All power flow solutions that correspond to the point $P_g^C = \lambda P_g^A + (1 - \lambda) P_g^B$, $V^C = \lambda V^A + (1 - \lambda) V^B$ are infeasible for the OPF constraints (1b)–(1i).

The method in [9] uses local optimization solvers to seek such points A, B, and C for a given OPF problem.

B. Proposed Algorithm for Certifying Disconnectedness

If the method from [9] succeeds, the resulting points A, B, and C identify a non-convexity in the OPF feasible space. Since a disconnected region is necessarily non-convex, the points A, B, and C may (but do not necessarily) indicate disconnectedness. To certify disconnectedness, we seek to further show that the feasible points A and B are separated by a hyperplane on which all points are infeasible with respect to the OPF constraints (1b)–(1i), including voltage, reactive power, and flow limits. In that case, since all feasible paths
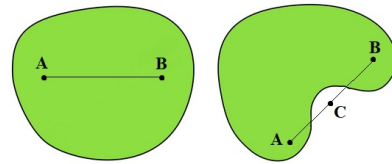

Figure 1. Illustrations of convex and non-convex feasible regions. On the left, all points along the line segment between feasible points A and B are feasible. This is true for all possible pairs of feasible points. In contrast, on the right, the infeasible point C is on the line between points A and B. Points A, B, and C confirm non-convexity of this region.

between points A and B must pass through this hyperplane, no feasible path exists and the points A and B thus belong to different disconnected components of the OPF feasible space.

(a)
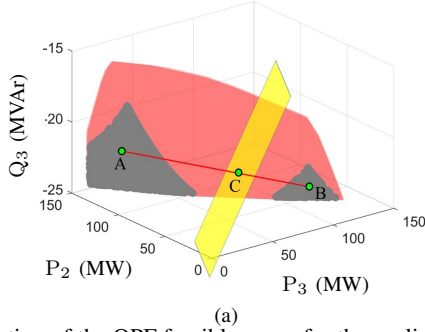
(a) A projection of the OPF feasible space for the cyclic 3-bus system in [8]. The proposed algorithm certifies the space's disconnectedness.

(b)
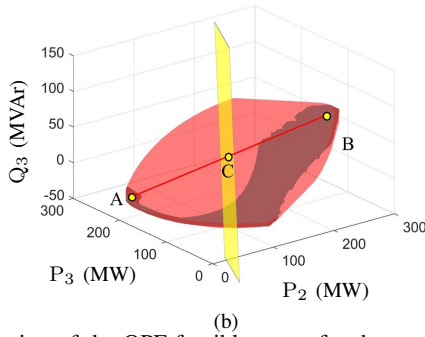
(b) A projection of the OPF feasible space for the acyclic 3-bus test case in [8]. The OPF feasible space is non-convex but connected, and the proposed algorithm does not certify disconnectedness.

Figure 2. Illustrative examples of applying the proposed algorithm to two test cases from [8]. The OPF feasible spaces, which are computed using the method in [1], are shown in gray. The pink regions correspond to the QC relaxation's feasible spaces (without bound tightening). The method from [9] identifies non-convexities in both feasible spaces via the feasible points A and B and the infeasible point C on the line connecting A and B. The yellow hyperplane is normal to the line connecting A and B and passes through point C. Applying bound tightening to (10) certifies infeasibility of all points on the yellow hyperplane in Fig. 2a, and thus this feasible space is disconnected. Conversely, the OPF problem's feasible space intersects the yellow hyperplane in Fig. 2b and thus (10) is feasible. Accordingly, the proposed algorithm does not certify disconnectedness of this OPF feasible space.

While any separating hyperplane would suffice, we leverage knowledge regarding the infeasibility of point C by selecting the hyperplane perpendicular to the line segment between points A and B that passes through point C. This ensures that at least one point on the hyperplane is infeasible. Note that our numerical results in Section V also consider various rotations when the hyperplane that is perpendicular to the line between points A and B fails to certify disconnectedness.

To certify infeasibility for all points on the hyperplane, we formulate a feasibility problem consisting of the OPF problem's constraints (1b)–(1i) augmented with an additional constraint corresponding to the hyperplane. We then apply the QC relaxation to the constraints (1b)–(1i) as described in Section III-A to obtain the set of constraints

$$\text{(8b)–(8h) and } n^\top \begin{bmatrix} P_g - P_g^C \\ \hat{w} - (V^C)^2 \end{bmatrix} = 0, \qquad (10)$$

where n is the vector for the line between points A and B, i.e., $n = \begin{bmatrix} P_g^A - P_g^B \\ (V^A)^2 - (V^B)^2 \end{bmatrix}$, and $\hat{w}$ denotes the vector consisting of w_{ii} for all $i \in \mathcal{G}$ corresponding to the squared

voltage magnitudes at each generator bus. Since the restriction to the hyperplane is a linear constraint, (10) is an SOCP. While the separating hyperplane itself is defined in terms of active power generation and squared voltage magnitudes, the proposed algorithm enforces *all* OPF constraints, including those involving load-bus voltages, phase angles, reactive power injections, and line flows. In other words, the feasibility problem (10) augments the OPF constraints (8b)–(8h) with the separating hyperplane constraint such that the resulting disconnectedness certificates consider all OPF constraints.

Infeasibility of (10) guarantees that all points on the hyperplane are infeasible. Applying bound tightening techniques, as described in Section III-B, identifies cases where the relaxed formulation (10) is infeasible, thus certifying the disconnectedness for the corresponding OPF feasible spaces. Conversely, if applying bound tightening to (10) does not prove infeasibility, then the test for disconnectedness is indeterminate. Rotating the hyperplane in (10) may help certify infeasibility in such cases, as shown numerically in Section V via ad hoc rotations.

To illustrate the proposed algorithm, Fig. 2 visualizes results from two three-bus test cases from [8]. In Fig. 2a, the proposed algorithm certifies that the OPF feasible space is disconnected via infeasibility of (10) for the yellow hyperplane, after bound tightening. Conversely, the OPF feasible space in Fig. 2b is non-convex but connected. Accordingly, the algorithm does not certify disconnectedness since the yellow plane passes through the OPF feasible space, and thus (10) is feasible.

Fig. 3 shows another example using the nine-bus system from [7] which has a feasible space with three disconnected components. The method from [9] identifies points A and B as feasible with the infeasible point C on the connecting line segment. In this example, the normal hyperplane at point C, shown in yellow, does not certify disconnectedness as it passes through the third disconnected component of the feasible space in the lower-left corner of the figure. Conversely, applying bound tightening using the green hyperplane, which rotates the yellow hyperplane by $45°$ around the P_2 axis, does certify disconnectedness of the feasible space.

This particular rotation was identified via trial and error. Future work will focus on developing a margin-maximizing orientation strategy to automate the selection of the separating hyperplane. Instead of using manual rotations, as in Fig. 3, this approach will treat the hyperplane's orientation as an optimization variable and search for the direction that maximizes an infeasibility measure, such as the minimum aggregate violation of the OPF constraints on the QC-relaxed feasibility problem. A hierarchical coarse-to-fine search, combining a broad grid scan with local derivative-free refinement, could help find the orientation that provides the largest infeasibility margin, thereby improving the algorithm's robustness.

The comparison in Table I emphasizes the fundamental differences between existing feasible path algorithms and the proposed disconnectedness-certifying approach. While prior literature [11]–[13] focus on constructing feasible transition paths between operating points, none can rigorously determine when such a path does not exist. To the best of our knowledge, our proposed algorithm is the first and only algorithm

Table I
COMPARISON BETWEEN FEASIBLE PATH ALGORITHMS AND THE PROPOSED DISCONNECTEDNESS-CERTIFYING ALGORITHM

| Ref.	Certifies Disconnectedness	Identifies a Feasible Path	Optimizes Control Actions	Core Principle
[11]	✗	✓	✗	Uses sequential convex restrictions to trace feasible paths between operating points.
[12]	✗	✓	✓	Sequentially adjusts controls using Lagrange multiplier sensitivities to minimize losses.
[13]	✗	✓	✓	Finds a discretized shortest path via a nonlinear program that minimizes control actuations.
Proposed Algorithm	✓	✗	✗	Certifies disconnectedness by proving infeasibility of all points on a separating hyperplane.
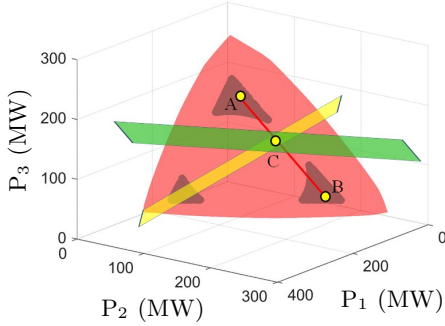
Figure 3. Feasible space projection for the 9-bus test system from [7]. Although the OPF problem's feasible space shown by the gray regions is disconnected, the proposed algorithm fails to certify disconnectedness since the yellow plane that is normal to the line segment between point A and B passes through the component of the feasible space in the lower-left corner of the figure. Conversely, applying bound tightening to the green hyperplane which is rotated by $45°$ around the P_2 axis certifies disconnectedness.

Table II
RESULTS FOR CHECKING THE FEASIBILITY OF TRANSITIONING BETWEEN DIFFERENT POINTS IN VARIOUS TEST CASES.

Test Cases	Rotation Angles	Disconnected Feasible Space
Cyclic 3-bus [8]	$(0°, 0°, 0°)$	Yes
5-bus [8]	$(0°, 0°, 0°)$	Yes
5-bus [7]	$(0°, 0°, 0°)$	Yes
9-bus [7]	$(0°, 45°, 0°)$	Yes
14-bus-sad [25]	$(0°, 0°, 0°)$	Yes
30-bus-ieee [25]	$(0°, 0°, 0°)$	Yes
118-bus-api [7]	$(0°, 0°, 0°)$	Yes

capable of certifying the disconnectedness of an OPF feasible space. Thus, the proposed approach complements existing path-finding methods by definitely certifying when feasible transitions between operating points are impossible.

V. NUMERICAL RESULTS

This section summarizes numerical results from applying the proposed algorithm to challenging OPF test cases from [7], [8], [25]. These numerical studies were performed on a computer with a 3.3 GHz Intel Core i7 processor and 16 GB of RAM. The proposed algorithm is implemented in MATLAB using YALMIP (R2023.09) [26] and solved using MOSEK (10.0.46). Default interior-point settings were employed, with primal/dual feasibility and relative/absolute optimality gap tolerances of 10^{-6}. For the optimization-based bound-tightening procedure, the algorithm was executed iteratively until no variable bound improved beyond 10^{-4} p.u. for power injections and 10^{-5} p.u. for voltage magnitudes.

Table II shows selected results obtained by applying the proposed algorithm to different test cases. The proposed algorithm identifies disconnectedness for several test cases, ranging from very small to mid-size systems. For the small cases, visualizing the feasible spaces as in [8] (see Figs. 2a and 3 for two examples) corroborates the disconnectedness certificates from our proposed algorithm. For the test cases in Table II, the voltage phasors for the feasible points which belong to different disconnected components of the feasible space are given in the appendix. These test cases are known to challenge OPF solution algorithms, with many relaxations of these problems yielding large relaxation gaps and/or local solvers finding suboptimal local solutions. This is consistent with our expectation that OPF algorithms often struggle with problems that have disconnected feasible spaces.

For other test cases, the proposed algorithm returned an indeterminate result, i.e., did not certify disconnectedness of the OPF feasible spaces. We note that this does not necessarily indicate that the feasible spaces for these problems are connected. Different combinations of points A, B, and C and/or different orientations of the candidate separating hyperplanes may potentially be able to certify disconnectedness, as our condition is sufficient but not necessary.

Our algorithm does not certify disconnectedness for many PGLib test cases [11], which suggests but does not guarantee that their feasible spaces may be connected. We know from the feasible path algorithm in [11] that feasible paths exist between certain pairs of operating points considered in that paper for systems such as "57-bus-ieee" and "118-bus". However, our indeterminate result means that it is unclear whether the feasible spaces for these problems are indeed connected everywhere or if the pairs of operating points in [11] happen to be in the same component of a disconnected feasible space.

Lastly, we discuss the computational aspects of the proposed algorithm. The most computationally demanding step is the application of optimization-based bound tightening to certify infeasibility of (10). However, for all the OPF problems we tested, the bound tightening step was not computationally intensive relative to typical bound tightening applications such as global solution methods for OPF problems [18]–[21]. In our algorithm, the bound-tightening step typically requires only a few iterations to either certify the infeasibility of transitioning between the candidate operating points or terminate without certification. For example, the algorithm certifies the disconnectedness for the "118-bus-api" test case in approximately six minutes, whereas traditional optimization-based bound-tightening methods applied in global OPF solvers often require substantially longer runtimes, on the order of hours, for

Table III
VOLTAGES FOR POINTS A AND B FOR THE 3-BUS TEST SYSTEM IN [8].

	Point A	Point B
1	0.8962 - 0.0919i	0.8846 - 0.1660i
2	0.9040 + 0.0000i	0.9996 + 0.0000i
3	1.0282 + 0.0888i	0.9278 - 0.0740i

Table IV
CORRESPONDING VOLTAGES FOR POINTS A AND B FOR THE 5-BUS TEST
SYSTEM IN [8].

Bus	Point A	Point B
1	0.9184 - 0.1354i	0.8463 - 0.3785i
2	0.9030 - 0.1643i	0.8436 - 0.4049i
3	0.9878 + 0.0000i	1.0878 + 0.0000i
4	0.9040 - 0.1524i	0.8370 - 0.3940i
5	1.0495 + 0.2700i	0.9428 - 0.2943i

systems of comparable size. Recent bound-tightening advances have further improved scalability, making such techniques tractable even for large OPF problems [27], [28]. Moreover, unlike conventional bound tightening settings, the proposed algorithm can certify transition infeasibility within only a few iterations, maintaining computational efficiency for relatively large systems. We attribute this to the fact that the feasibility problem (10) restricts the QC relaxation to a hyperplane rather than the entire OPF feasible space. Future work will incorporate more scalable bound-tightening and parallel computing approaches [27], [28] to further improve tractability.

VI. CONCLUSION

This paper presents an algorithm for certifying the presence of disconnected components in the feasible spaces of OPF problems. The algorithm identifies candidate operating points that may lie in different components and employs the QC relaxation with bound tightening to verify that all points on a separating hyperplane are infeasible. When infeasibility is confirmed, the two operating points are proven to belong to distinct disconnected components, indicating that no feasible path exists between them. To the best of our knowledge, this is the first algorithm capable of rigorously certifying disconnectedness in OPF feasible spaces. Understanding whether non-convexities correspond to disconnected components enhances both theoretical insights into OPF feasible space geometry and the reliability of power system operations, with practical implications by enabling feasible-space decomposition, contingency-aware dispatch, and secure operating point selection. Future work will focus on developing systematic methods for selecting the optimal rotation of the separating hyperplane and integrating this approach with feasible path algorithms.

APPENDIX

Tables II–VIII provide the voltage phasors for points A and B which our proposed algorithm identifies as belonging to different disconnected components of the corresponding OPF problems' feasible spaces.

Table V
VOLTAGES FOR POINTS A AND B FOR THE 5-BUS TEST SYSTEM IN [7].

	Point A	Point B
1	1.0467 - 0.0000i	1.0500 - 0.0000i
2	0.9550 - 0.0578i	0.9838 - 0.1183i
3	0.9485 - 0.0533i	0.9796 - 0.1196i
4	0.7791 + 0.6011i	0.9931 - 0.1650i
5	0.7362 + 0.7487i	1.0317 - 0.1032i

Table VI
VOLTAGES FOR POINTS A AND B FOR THE 9-BUS TEST SYSTEM IN [7].

	Point A	Point B
1	0.9025 + 0.0000i	0.9058 + 0.0000i
2	0.9042 - 0.1541i	0.9220 + 0.0789i
3	0.9063 - 0.1819i	0.9082 + 0.2334i
4	0.9052 - 0.0927i	0.9089 - 0.0063i
5	0.8961 - 0.1606i	0.9103 + 0.0105i
6	0.9082 - 0.1888i	0.9297 + 0.1444i
7	0.8934 - 0.2080i	0.9246 + 0.0647i
8	0.9034 - 0.1787i	0.9275 + 0.0545i
9	0.8848 - 0.1644i	0.8995 - 0.0302i

REFERENCES

[1] D. K. Molzahn, "Computing the Feasible Spaces of Optimal Power Flow Problems," *IEEE Trans. Power Syst.*, vol. 32, no. 6, pp.4752–4763, 2017.

[2] D. Bienstock and A. Verma, "Strong NP-Hardness of AC Power Flows Feasibility," *Oper. Res. Lett.*, vol. 47, no. 6, pp. 494–501, 2019.

[3] J. Momoh, R. Adapa, and M. El-Hawary, "A Review of Selected Optimal Power Flow Literature to 1993. Parts I and II," *IEEE Trans. Power Syst.*, vol. 14, no. 1, pp. 96–111, Feb. 1999.

[4] D. K. Molzahn and I. A. Hiskens, "A Survey of Relaxations and Approximations of the Power Flow Equations," *Found. Trends Electric Energy Syst.*, vol. 4, no. 1-2, pp. 1–221, Feb. 2019.

[5] B. C. Lesieutre and I. A. Hiskens, "Convexity of the Set of Feasible Injections and Revenue Adequacy in FTR Markets," *IEEE Trans. Power Syst.*, vol. 20, no. 4, pp. 1790–1798, Nov. 2005.

[6] B. Zhang and D. Tse, "Geometry of Feasible Injection Region of Power Networks," in *49th Ann. Allerton Conf. Commun., Control, Comput. (Allerton)*, Sept. 2011, pp. 1508–1515.

[7] W. Bukhsh, A. Grothey, K. McKinnon, and P. Trodden, "Local Solutions of the Optimal Power Flow Problem," *IEEE Trans. Power Syst.*, vol. 28, no. 4, pp. 4780–4788, 2013.

[8] M. R. Narimani, D. K. Molzahn, D. Wu, and M. L. Crow, "Empirical Investigation of Non-Convexities in Optimal Power Flow Problems," in *American Control Conf. (ACC)*, 2018, pp. 3847–3854.

[9] D. K. Molzahn, "Identifying and Characterizing Non-Convexities in Feasible Spaces of Optimal Power Flow Problems," *IEEE Trans. Circuits Syst. II: Exp. Briefs*, vol. 65, no. 5, pp. 672–676, May 2018.

Table VII
VOLTAGES FOR POINTS A AND B FOR PGLIB 14-BUS-IEEE-SAD.

Bus	Point A	Point B
1	1.0600 + 1.1758i	1.0600 + 0i
2	1.0348 - 0.0785i	1.0351 - 0.0785i
3	0.9930 - 0.2185i	0.9745 - 0.2108i
4	0.9967 - 0.1730i	0.9923 - 0.1718i
5	1.0028 - 0.1470i	1.0001 - 0.1465i
6	1.0290 - 0.2546i	1.0289 - 0.2551i
7	1.0180 - 0.2339i	1.0160 - 0.2333i
8	1.0331 - 0.2373i	1.0331 - 0.2372i
9	1.0080 - 0.2617i	1.0061 - 0.2611i
10	1.0031 - 0.2637i	1.0015 - 0.2633i
11	1.0120 - 0.2607i	1.0110 - 0.2606i
12	1.0102 - 0.2663i	1.0100 - 0.2667i
13	1.0049 - 0.2663i	1.0045 - 0.2665i
14	0.9842 - 0.2767i	0.9830 - 0.2765i

Table VIII
VOLTAGES FOR POINTS A AND B FOR PGLIB 30-BUS-IEEE.

Bus	Point A	Point B
1	1.0600 +0i	1.0600 + 0i
2	1.0405 - 0.0707i	1.0350 - 0.0687i
3	1.0077 - 0.1168i	1.0081 - 0.1174i
4	0.9935 - 0.1422i	0.9940 - 0.1429i
5	0.9816 - 0.2249i	0.9805 - 0.2248i
6	0.9841 - 0.1698i	0.9875 - 0.1721i
7	0.9739 - 0.2000i	0.9755 - 0.2013i
8	0.9760 - 0.1803i	0.9857 - 0.1856i
9	1.0088 - 0.2315i	1.0088 - 0.2334i
10	0.9973 - 0.2591i	0.9957 - 0.2608i
11	1.0332 - 0.2371i	1.0327 - 0.2390i
12	1.0149 - 0.2510i	1.0074 - 0.2492i
13	1.0290 - 0.2545i	1.0133 - 0.2507i
14	0.9959 - 0.2630i	0.9891 - 0.2616i
15	0.9907 - 0.2631i	0.9847 - 0.2623i
16	0.9988 - 0.2572i	0.9937 - 0.2571i
17	0.9918 - 0.2611i	0.9891 - 0.2622i
18	0.9778 - 0.2707i	0.9733 - 0.2709i
19	0.9742 - 0.2727i	0.9705 - 0.2734i
20	0.9789 - 0.2702i	0.9758 - 0.2711i
21	0.9832 - 0.2638i	0.9814 - 0.2655i
22	0.9838 - 0.2638i	0.9820 - 0.2653i
23	0.9781 - 0.2666i	0.9737 - 0.2667i
24	0.9710 - 0.2674i	0.9690 - 0.2686i
25	0.9692 - 0.2586i	0.9695 - 0.2610i
26	0.9499 - 0.2612i	0.9503 - 0.2635i
27	0.9775 - 0.2509i	0.9794 - 0.2538i
28	0.9773 - 0.1796i	0.9818 - 0.1824i
29	0.9524 - 0.2670i	0.9543 - 0.2698i
30	0.9368 - 0.2787i	0.9388 - 0.2815i

[10] H. D. Chiang and C. Y. Jiang, "Feasible Region of Optimal Power Flow: Characterization and Applications," *IEEE Trans. Power Syst.*, vol. 33, no. 1, pp. 236–244, Jan. 2018.

[11] D. Lee, K. Turitsyn, D. K. Molzahn, and L. A. Roald, "Feasible Path Identification in Optimal Power Flow with Sequential Convex Restriction," *IEEE Trans. Power Syst.*, vol. 35, no. 5, pp. 3648–3659, Sept. 2020.

[12] R. M. Barros, G. G. Lage, and R. d. A. L. Rabêlo, "Sequencing Paths of Optimal Control Adjustments Determined by the Optimal Reactive Dispatch via Lagrange Multiplier Sensitivity Analysis," *European J. Oper. Res.*, vol. 301, no. 1, pp. 373–385, 2022.

[13] D. Turizo, D. Cifuentes, A. Leykin, and D. K. Molzahn, "Discrete Shortest Paths in Optimal Power Flow Feasible Regions," *IEEE Trans. Power Syst.*, vol. 40, no. 6, pp. 5027–5040, Nov. 2025.

[14] F. Capitanescu and L. Wehenkel, "Redispatching Active and Reactive Powers Using a Limited Number of Control Actions," *IEEE Trans. Power Syst.*, vol. 26, no. 3, pp. 1221–1230, 2011.

[15] D. T. Phan and X. A. Sun, "Minimal Impact Corrective Actions in Security-Constrained Optimal Power Flow Via Sparsity Regularization," *IEEE Trans. Power Syst.*, vol. 30, no. 4, pp. 1947–1956, 2015.

[16] D. Lee, K. Turitsyn, D. K. Molzahn, and L. A. Roald, "Feasible path identification in optimal power flow with sequential convex restriction," *IEEE Trans. Power Syst.*, vol. 35, no. 5, pp. 3648–3659, 2020.

[17] C. Coffrin, H. Hijazi, and P. Van Hentenryck, "The QC Relaxation: A Theoretical and Computational Study on Optimal Power Flow," *IEEE Trans. Power Syst.*, vol. 31, no. 4, pp. 3008–3018, July 2016.

[18] C. Coffrin, H. L. Hijazi, and P. Van Hentenryck, "Strengthening the SDP Relaxation of AC Power Flows with Convex Envelopes, Bound Tightening, and Valid Inequalities," *IEEE Trans. Power Syst.*, vol. 32, no. 5, pp. 3549–3558, Sept. 2017.

[19] B. Kocuk, S. S. Dey, and X. A. Sun, "Strong SOCP Relaxations for the Optimal Power Flow Problem," *Oper. Res.*, vol. 64, no. 6, pp. 1177–1196, May 2016.

[20] C. Chen, A. Atamtürk, and S. Oren, "Bound Tightening for the Alternating Current Optimal Power Flow Problem," *IEEE Trans. Power Syst.*, vol. 31, no. 5, pp. 3729–3736, Sept. 2016.

[21] B. Kocuk, S. S. Dey, and X. A. Sun, "Matrix Minor Reformulation and SOCP-Based Spatial Branch-and-Cut Method for the AC Optimal Power Flow Problem," *Math. Prog. Comput.*, vol. 10, no. 4, pp. 557–596, 2018.

[22] R. Zimmerman, C. Murillo-Sánchez, and R. Thomas, "MATPOWER: Steady-State Operations, Planning, and Analysis Tools for Power Systems Research and Education," *IEEE Trans. Power Syst.*, no. 99, pp. 1–8, 2011.

[23] R. Jabr, "Radial Distribution Load Flow using Conic Programming," *IEEE Trans. Power Syst.*, vol. 21, no. 3, pp. 1458–1459, Aug. 2006.

[24] G. McCormick, "Computability of Global Solutions to Factorable Nonconvex Programs: Part I–Convex Underestimating Problems," *Math. Prog.*, vol. 10, no. 1, pp. 147–175, 1976.

[25] IEEE PES Task Force on Benchmarks for Validation of Emerging Power System Algorithms, "The Power Grid Library for Benchmarking AC Optimal Power Flow Algorithms," *arXiv:1908.02788*, Aug. 2019. [Online]. Available: https://github.com/power-grid-lib/pglib-opf

[26] J. Lofberg, "YALMIP: A Toolbox for Modeling and Optimization in MATLAB," in *IEEE Int. Symp. Comput. Aided Control Sys. Design (CACSD)*, 2004, pp. 284–289.

[27] D. Shchetinin, T. T. De Rubira, and G. Hug, "Efficient Bound Tightening Techniques for Convex Relaxations of AC Optimal Power Flow," *IEEE Trans. Power Syst.*, vol. 34, no. 5, pp. 3848–3857, 2019.

[28] F. Cengil, H. Nagarajan, R. Bent, S. Eksioglu, and B. Eksioglu, "Learning to Accelerate Tightening of Convex Relaxations of the AC Optimal Power Flow Problem," *Comput. Optimiz. Appl. (*to appear*)*, 2025.

Table IX

VOLTAGES FOR POINTS A AND B FOR PGLIB 118-BUS-API.

Bus	Point A	Point B	Bus	Point A	Point B
1	1.0197 + 0.2895i	1.0155 + 0.3040i	60	0.9462 + 0.1948i	0.9256 + 0.1967i
2	0.9970 + 0.3292i	0.9849 + 0.3437i	61	0.9459 + 0.2144i	0.9257 + 0.2162i
3	1.0049 + 0.3088i	0.9985 + 0.3230i	62	0.9480 + 0.1671i	0.9317 + 0.1728i
4	0.9918 + 0.3741i	0.9865 + 0.3879i	63	0.9396 + 0.2273i	0.9199 + 0.2274i
5	0.9710 + 0.3807i	0.9745 + 0.3942i	64	0.9559 + 0.2148i	0.9457 + 0.2154i
6	1.0001 + 0.3511i	0.9948 + 0.3660i	65	1.0004 + 0.1966i	1.0157 + 0.1954i
7	0.9952 + 0.3558i	0.9854 + 0.3705i	66	1.0015 + 0.1488i	1.0038 + 0.1759i
8	0.9065 + 0.4304i	0.9036 + 0.4427i	67	0.9720 + 0.1310i	0.9661 + 0.1480i
9	0.8068 + 0.6162i	0.8014 + 0.6266i	68	0.9952 + 0.0880i	1.0025 + 0.0886i
10	0.6687 + 0.7912i	0.6608 + 0.7992i	69	0.9918 + 0i	0.9932 + 0i
11	0.9820 + 0.3455i	0.9698 + 0.3594i	70	1.0461 - 0.1712i	1.0462 - 0.1706i
12	0.9867 + 0.3744i	0.9694 + 0.3890i	71	1.0484 - 0.1566i	1.0485 - 0.1560i
13	0.9665 + 0.2559i	0.9571 + 0.2686i	72	1.0577 - 0.0705i	1.0577 - 0.0610i
14	0.9784 + 0.2891i	0.9655 + 0.3024i	73	1.0476 - 0.1591i	1.0477 - 0.1585i
15	0.9506 + 0.1009i	0.9491 + 0.1109i	74	0.9190 - 0.1975i	0.9191 - 0.1971i
16	0.9756 + 0.2856i	0.9635 + 0.2985i	75	0.9404 - 0.1802i	0.9398 - 0.1795i
17	0.9610 + 0.1708i	0.9590 + 0.1809i	76	0.9118 - 0.2284i	0.9118 - 0.2284i
18	0.9824 + 0.0856i	0.9746 + 0.0963i	77	1.0029 - 0.1090i	0.9940 - 0.1040i
19	0.9805 + 0.0584i	0.9789 + 0.0682i	78	0.9954 - 0.1175i	0.9863 - 0.1126i
20	0.9744 + 0.0282i	0.9701 + 0.0363i	79	0.9977 - 0.1091i	0.9885 - 0.1041i
21	0.9753 + 0.0326i	0.9689 + 0.0397i	80	1.0267 - 0.0427i	1.0174 - 0.0369i
22	0.9865 + 0.0600i	0.9774 + 0.0661i	81	0.9840 + 0.0394i	0.9852 + 0.0422i
23	1.0118 + 0.1318i	0.9986 + 0.1366i	82	0.9893 - 0.0722i	0.9813 - 0.0666i
24	1.0254 + 0.0610i	1.0174 + 0.0640i	83	1.0056 - 0.0405i	0.9998 - 0.0346i
25	1.0008 + 0.2774i	0.9841 + 0.2838i	84	1.0353 + 0.0245i	1.0332 + 0.0309i
26	0.8751 + 0.3432i	0.9534 + 0.3781i	85	1.0580 + 0.0662i	1.0575 + 0.0729i
27	1.0509 + 0.1388i	1.0505 + 0.1414i	86	1.0261 + 0.1930i	1.0249 + 0.1995i
28	1.0130 + 0.1834i	0.9950 + 0.1870i	87	0.9539 + 0.4622i	0.9510 + 0.4681i
29	0.9784 + 0.2605i	0.9408 + 0.2660i	88	1.0028 + 0.1004i	0.9916 + 0.1087i
30	0.9333 + 0.2433i	0.9453 + 0.2582i	89	0.9751 + 0.1814i	0.9561 + 0.1915i
31	0.9695 + 0.3026i	0.9249 + 0.3099i	90	0.9671 + 0.0070i	0.9484 + 0.0141i
32	0.9892 + 0.1511i	0.9655 + 0.1561i	91	0.9550 + 0.0357i	0.9390 + 0.0425i
33	0.9871 + 0.0101i	0.9876 + 0.0205i	92	0.9688 + 0.0850i	0.9517 + 0.0934i
34	1.0587 - 0.0525i	1.0592 - 0.0408i	93	0.9613 - 0.0417i	0.9462 + 0.0491i
35	1.0552 - 0.0668i	1.0562 - 0.0552i	94	0.9627 + 0.0187i	0.9495 + 0.0256i
36	1.0579 - 0.0674i	1.0585 - 0.0557i	95	0.9544 - 0.0261i	0.9423 - 0.0199i
37	1.0537 - 0.0393i	1.0558 - 0.0281i	96	0.9742 - 0.0484i	0.9636 - 0.0425i
38	0.9781 + 0.0907i	0.9855 + 0.1009i	97	0.9939 - 0.0562i	0.9839 - 0.0505i
39	1.0074 - 0.1595i	1.0116 - 0.1490i	98	0.9965 - 0.0230i	0.9856 - 0.0168i
40	0.9980 - 0.2053i	1.0031 - 0.1951i	99	1.0412 + 0.0328i	0.9385 + 0.0537i
41	0.9641 - 0.2171i	0.9686 - 0.2068i	100	0.9789 + 0.1096i	0.9654 + 0.1178i
42	0.9230 - 0.1778i	0.9250 - 0.1670i	101	0.9609 + 0.0704i	0.9458 + 0.0781i
43	1.0220 - 0.0402i	1.0221 - 0.0287i	102	0.9654 + 0.0769i	0.9489 + 0.0850i
44	0.9930 + 0.0482i	0.9917 + 0.0597i	103	0.9633 + 0.0269i	0.9292 + 0.1419i
45	0.9817 + 0.1064i	0.9797 + 0.1179i	104	0.9818 - 0.1019i	0.9626 - 0.0061i
46	1.0142 + 0.3083i	1.0105 + 0.3200i	105	0.9713 - 0.1393i	0.9518 - 0.0323i
47	0.9830 + 0.1464i	0.9804 + 0.1567i	106	0.9560 - 0.1421i	0.9603 - 0.0606i
48	0.9764 + 0.1470i	0.9732 + 0.1589i	107	0.9584 - 0.2309i	1.0458 - 0.1728i
49	0.9648 + 0.1224i	0.9615 + 0.1343i	108	0.9504 - 0.1871i	0.9554 - 0.0420i
50	0.9564 + 0.1053i	0.9541 + 0.1123i	109	0.9424 - 0.2058i	0.9572 - 0.0450i
51	0.9418 + 0.0853i	0.9411 + 0.0862i	110	0.9286 - 0.2463i	0.9678 - 0.0429i
52	0.9371 + 0.0738i	0.9372 + 0.0730i	111	0.9286 - 0.2463i	0.9384 + 0.0553i
53	0.9406 + 0.0943i	0.9431 + 0.0889i	112	0.8845 - 0.3181i	0.9741 - 0.1373i
54	0.9587 + 0.1589i	0.9634 + 0.1500i	113	0.9243 + 0.1710i	0.9227 + 0.1797i
55	0.9562 + 0.1386i	0.9552 + 0.1313i	114	1.0111 + 0.1300i	0.9972 + 0.1338i
56	0.9561 + 0.1433i	0.9566 + 0.1358i	115	1.0151 + 0.1278i	1.0030 + 0.1314i
57	0.9533 + 0.1152i	0.9526 + 0.1138i	116	1.0024 + 0.0805i	1.0096 + 0.0812i
58	0.9453 + 0.1012i	0.9450 + 0.0985i	117	0.9825 + 0.3273i	0.9660 + 0.3413i
59	0.9430 + 0.2561i	0.9051 + 0.2539i	118	0.9158 - 0.2145i	0.9155 - 0.2141i